Journal of Hazardous Materials 512 (2026) 142316

Contents lists available at ScienceDirect

Journal of Hazardous Materials

journal homepage: www.elsevier.com/locate/jhazmat

H3K18 lactylation-regulated ATG10 is involved in the acute respiratory distress syndrome induced by acute exposure to hydrogen sulfide through activation of autophagy in lung epithelial cells

Bingyu Ling [a,b,c,1], Ping Geng [b,1], Bowen Fan [c,1], Xiaolong Wu [a], Yi Yang [c], Jiaheng Lin [c], Wenjie Li [c], Qizhan Liu [c], Cheng Cheng [c,*], Jinsong Zhang [a,c,**], Hao Wu [a,c,**]

[a] Department of Emergency Medicine, The First Affiliated Hospital with Nanjing Medical University, Jiangsu Province Hospital, Nanjing 210029, Jiangsu, People's Republic of China
[b] Department of Emergency Medicine, Northern Jiangsu People's Hospital Affiliated to Yangzhou University, Yangzhou 225001, Jiangsu, People's Republic of China
[c] Center for Global Health, The Key Laboratory of Modern Toxicology, Ministry of Education, School of Public Health, Nanjing Medical University, Nanjing 211166, Jiangsu, People's Republic of China

HIGHLIGHTS

- Acute exposure to H_2S induces ARDS through disruption of lung epithelial barrier via autophagy of lung epithelial cells.
- Glycolysis-derived, H3K18la-regulated ATG10 is involved in H_2S-induced autophagy of lung epithelial cells.
- DCA blocks H_2S-induced ARDS by inhibiting glycolysis and lung epithelial cell autophagy via H3K18la-regulated ATG10.

GRAPHICAL ABSTRACT

In alveolar epithelial cells, H_2S causes elevation of glycolysis, which leads to the accumulation of lactate. Lactate accumulation induces modifications of H3K18 lactylation, thereby promoting transcription of the ATG10 gene, resulting in activation of autophagy in alveolar epithelial cells, which in turn disrupts the alveolar epithelial barrier and thereby triggers the acute respiratory distress syndrome (ARDS). DCA via inhibition of glycolysis or the activation of ATG10 alleviates these pathological effects induced by H_2S, which blocks H_2S-induced ARDS.

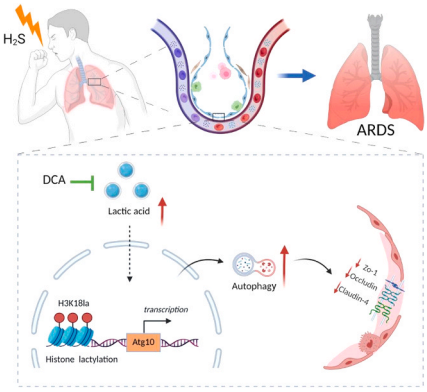

* Corresponding author.
** Corresponding authors at: Department of Emergency Medicine, The First Affiliated Hospital with Nanjing Medical University, Jiangsu Province Hospital, Nanjing 210029, Jiangsu, People's Republic of China.
E-mail addresses: drchengcheng@njmu.edu.cn (C. Cheng), zhangjso@njmu.edu.cn (J. Zhang), drwuhao@njmu.edu.cn (H. Wu).
[1] Authors contributed equally.

https://doi.org/10.1016/j.jhazmat.2026.142316
Received 21 January 2026; Received in revised form 18 April 2026; Accepted 4 May 2026
Available online 7 May 2026

ARTICLE INFO

Keywords:
Hydrogen sulfide
Acute respiratory distress syndrome
H3K18 lactylation
Autophagy
Lung epithelial barrier

ABSTRACT

Hydrogen sulfide (H_2S) is a colorless, toxic, asphyxiant gas. In recent years, industrial accidents involving H_2S exposure have frequently resulted in fatalities and disabilities. Acute respiratory distress syndrome (ARDS) poses a substantial burden on healthcare systems worldwide. The syndrome's heterogeneity and multifaceted pathogenesis, combined with a paucity of effective treatments, contribute to a persistently high mortality rate, which currently stands at 30–35%. The present study utilized metabolomics, transcriptomics, and CUT&Tag sequencing to explore ARDS pathogenesis, providing insights into its mechanisms and therapeutic targets for its treatment. Serum metabolomics for individuals with H_2S-induced ARDS identified lactate accumulation as a pivotal metabolic event that mediates changes in H_2S-induced ARDS biomarkers. Lactate, a potential biomarker of H_2S-induced ARDS, is associated with a poor prognosis. However, whether elevated lactate directly promotes H_2S-induced ARDS and the mechanisms underlying this effect remain unclear. Here, we demonstrate that lactate disrupts the alveolar epithelial barrier, thereby facilitating the development of ARDS. Mechanistically, lactate promotes histone H3K18 lactylation at the promoter for ATG10, a gene involved in the process of autophagy, driving its transcription and upregulating autophagy in alveolar epithelial cells, which results in disruption of the epithelial barrier. For rats, the reduction of lactate generation by a glycolytic inhibitor mitigates H_2S-induced ARDS, as evidenced by attenuated pulmonary edema. Our results show that the lactate-autophagy axis mediates H_2S-induced ARDS. Therefore, targeting the regulation of lactate production and/or autophagy is a therapeutic strategy for patients with H_2S-induced ARDS.

1. Introduction

Hydrogen sulfide (H_2S), a common gaseous toxin and occupational hazard, poses escalating environmental and health risks due to its widespread industrial use and unavoidable environmental release. It is a cause of death resulting from fatal toxic gas exposure and constitutes a major threat to public health [1]. Currently, workers in more than 80 occupational categories are at risk of H_2S exposure [2]. Mass exposure events may trigger public health emergencies, posing substantial threats to human health. High concentrations H_2S (500–1000 ppm) inhibit cytochrome oxidase, leading to cellular asphyxiation and "lightning death". Lower concentrations (10–500 ppm) may cause varying degrees of respiratory damage, ranging from irritative inflammation of the upper airways to acute respiratory distress syndrome (ARDS) [3].

ARDS, an illness manifested as acute refractory hypoxemic respiratory failure, imposes a health burden due to its high prevalence, mortality, and disability rates. In recent years, progress has been made in the diagnosis and treatment of ARDS [4]. However, due to its heterogeneity, complex pathogenesis, and lack of effective therapeutic approaches (there is no specific medication, and issues such as ventilator-induced lung injury often arise during treatment), the global mortality rate remains at 30–35% [5]. In ARDS, damage to the barrier formed by alveolar epithelial and endothelial cells is a primary cause of respiratory dysfunction [4,6]. Disruption of the epithelial-endothelial barrier leads to the flooding of alveolar cavities with fluid, red blood cells, and leukocytes, thereby impairing gas exchange and causing respiratory failure [7,8]. Although injury to endothelial cells alone is insufficient to cause substantial pulmonary edema, structural and functional impairment of the alveolar epithelial barrier is a fundamental event in its development [9,10]. Tight junctions, intercellular connections located at the apical region of cell-cell contacts, are essential for regulating epithelial barrier permeability [11,12]. Further mechanistic studies are needed to develop therapeutic strategies and to identify new therapeutic targets for ARDS.

The inhalation of H_2S primarily injures alveolar epithelial cells, in which the ensuing barrier disruption constitutes a fundamental mechanism in the pathogenesis of H_2S-induced ARDS. Therefore, investigation of the alveolar epithelial barrier dysfunction, induced by structural damage to tight junctions, and its underlying mechanisms holds value for improving survival rates for H_2S-induced ARDS. Such investigations could lead to a breakthrough in the treatment of gas-induced ARDS.

Autophagy, a mechanism for programmed cell death, functions via the cytoplasmic lysosomal system to engulf and degrade damaged, denatured, or senescent cells; organelles; macromolecular proteins; and invading pathogens [13].This process facilitates "self-digestion" and maintains intracellular homeostasis [14]. Autophagy attenuates acute lung injury (ALI) by regulating inflammatory responses and apoptosis. For example, sevoflurane anesthesia activates protective autophagy via the AMPK-ULK1 pathway [15], which in turn inhibits lipopolysaccharide (LPS)-induced ALI. However, excessive activation of autophagy leads to cell injury. In sepsis-induced ALI models, the imbalance of autophagy, ferroptosis, and necroptosis is a key mechanism triggering lung injury [16]. Nonetheless, it is unclear if and how H_2S exposure regulates autophagy in the progression of ARDS.

A marked increase in glycolysis is a hallmark of glucose metabolic reprogramming and a driver in the progression of ARDS. For alveolar epithelial cells, a hypoxic environment induces glycolysis [17]. Its occurrence is regulated by a series of rate-limiting enzymes. Hexokinase 2 (HK2) phosphorylates glucose to glucose-6-phosphate. Enolase-1 (ENO-1), located downstream, catalyzes the dehydration of 2-phosphoglycerate to form phosphoenolpyruvate[18]. By catalyzing the reduction of pyruvate to lactate, lactate dehydrogenase A (LDHA) concurrently regenerates NAD^+ , thereby providing the cofactor required to sustain anaerobic glycolysis [19]. Lactate is the end product of glycolysis and a regulatory factor involved in the modulation of various signaling pathways [20–22]. However, research on the function of lactate at the molecular level remains scarce.

In 2019, Zhang et al. introduced the concept of lysine lactylation (Kla), a previously unrecognized functional role of lactate. Lactylation is a post-translational modification that uses lactate as a substrate to add a lactyl group to the lysine residues of proteins, thereby influencing protein localization, interactions, and stability, and regulating cellular functions [23]. Research on histone Kla reveals an epigenetic mechanism through which lactate contributes to disease pathogenesis [24]. As a manifestation of lactate's function, lactylation is involved in diverse physiological and pathological contexts, including chronic cardiovascular diseases, neural injury, inflammatory disorders, and tumor proliferation [25,26]. The potential involvement of lactylation in the pathogenesis of H_2S-induced ARDS remains to be investigated.

Here, we show that lactylation has a function in the pathogenesis of H_2S-induced ARDS. The underlying mechanisms include H_2S-triggered elevation of lactate levels and histone H3 lysine 18 lactylation (H3K18la), which subsequently activate ATG10-mediated autophagy, promoting disruption of the alveolar epithelial barrier. Inhibition of lactylation or silencing of ATG10 attenuates disruption of the pulmonary epithelial barrier, thereby revealing a potential target for the treatment of H_2S-induced ARDS. In sum, our results elucidate a previously unknown mechanism for H_2S-induced ARDS and offer therapeutic perspectives based on metabolic reprogramming.

2. Materials and methods

2.1. Human sample collection

Between 1 January 2018 and 30 December 2024, whole blood samples were collected within 12 h of admission from patients treated at Northern Jiangsu People's Hospital Affiliated to Yangzhou University, The First Affiliated Hospital with Nanjing Medical University, Liyang People's Hospital, and Yangzhou Hongquan Hospital. Blood samples from controls were collected from the physical examination center, Northern Jiangsu People's Hospital Affiliated to Yangzhou University.

In the present study, acute H_2S exposure is defined as a documented recent single episode of occupational or accidental inhalation exposure, followed by the rapid onset of clinical manifestations associated with acute poisoning and prompt medical attention. All patients with acute H_2S poisoning met the diagnostic criteria of GBZ 31–2002 (Diagnostic Criteria for Occupational Acute H_2S Poisoning), including: (1) a clear history of occupational exposure involving short-term inhalation of relatively high concentrations of H_2S; (2) acute clinical manifestations primarily involving the central nervous system and respiratory system; (3) confirmation through on-site occupational health investigations that the poisoning incident was consistent with H_2S exposure; (4) complete clinical and imaging data; and (5) exclusion of other causes of lung injury, including trauma, pulmonary infections caused by other etiologies, and pre-existing cardiopulmonary diseases (such as chronic bronchitis, interstitial pulmonary fibrosis, previous lung tumor surgery, pulmonary embolism, and heart disease).

Among patients with acute H_2S poisoning, those with ARDS were further diagnosed according to the global ARDS definition, based on the following criteria: (1) acute hypoxic respiratory failure occurring within 1 week of a known clinical trigger, or within 1 week of the onset or exacerbation of respiratory symptoms; (2) chest X-ray or computed tomography (CT) scan showing bilateral diffuse infiltrates that cannot be fully attributed to pleural effusion, atelectasis, or pulmonary nodules; (3) impaired oxygenation, defined as $PaO_2/FiO_2 \leq 300$ mmHg, or, when using a pulse oximeter, $SpO_2/FiO_2 \leq 315$ and $SpO_2 \leq 97\%$; for patients receiving high-flow nasal cannula oxygen therapy, the flow rate had to be ≥ 30 L/min, and the patient must have met the above oxygenation criteria; and (4) respiratory failure could not be entirely attributed to heart failure or fluid overload; where necessary, cardiogenic pulmonary edema must be ruled out through objective assessment.

Patients with incomplete clinical information, those with malignant tumors or tuberculosis, or those with unsuitable blood samples were excluded.

Based on the above criteria, the enrolled subjects were divided into three groups: a control group, an acute H_2S poisoning group without ARDS (H_2S group), and an acute H_2S poisoning group with ARDS (H_2S+ARDS group). A total of 20 controls, 17 patients in the H_2S group, and 15 patients in the H_2S+ARDS group were included. Relevant exposure characteristics, including H_2S exposure concentration, duration of exposure, and time from poisoning to presentation, are summarized in Supplementary Table S1. This study was approved by the Ethics Committee of Northern Jiangsu People's Hospital Affiliated to Yangzhou University, and written informed consent was obtained from all participants or their legal guardians.

2.2. Animals

The H_2S-induced ARDS model was developed with 6-week-old, SPF-grade male Sprague-Dawley (SD) rats via controlled inhalation exposure. The rats were obtained from the Animal Center of Nanjing Medical University and were housed under standard conditions for one week to allow for environmental acclimation prior to experimentation. All rats were provided *ad libitum* access to a standard laboratory diet and housed under a 12-hour light/12-hour dark cycle. The Animal Ethics Committee of Nanjing Medical University (IACUC-2311003) approved all animal procedures.

2.3. H_2S-induced ARDS model and dichloroacetate (DCA) intervention

Based on the methods described by our previous research [27], air was mixed with standard hydrogen sulfide gas (1% H_2S) using a flow controller in a specially designed, sealed, resin-glass exposure chamber with a volume of approximately 0.7 m^3 . The H_2S concentration within the exposure chamber was continuously monitored with an H_2S detector, and the airflow was adjusted to maintain the target exposure level. In this experiment, SD rats were acutely exposed to 0, 100, 200, or 300 ppm of H_2S in the chamber. To prevent hypoxia during exposure, air was intermittently supplied via a blower (5–8 min intervals). After 3 h of continuous exposure, the rats were removed from the chamber and allowed to breathe normally, awaiting further processing.

For DCA intervention, SD rats were exposed to 0 or 300 ppm H_2S in an acrylic exposure chamber for 3 h. After exposure, the animals were returned to fresh air. At 12 h after H_2S exposure, rats received an intraperitoneal injection of DCA or DMSO. After 24 h of exposure, the rats were subjected to related assessments, and arterial blood, serum, and lung tissues were collected for subsequent analyses.

2.4. Evans blue (EB) staining

EB dye was injected intravenously at a concentration of 2% (4 mL / kg) via the tail vein. One hour later, the rats were anesthetized and perfused via the right ventricle with 20 mL of saline for 2 min. The lung tissues were then excised, weighed, and homogenized in formamide (1 mL/100 mg) at 55 °C for 24 h. After centrifugation at 12,000 rpm for 20 min, the concentration of EB in the supernatant was determined spectrophotometrically at 620 nm.

2.5. Collection of bronchoalveolar lavage fluid (BALF)

Following anesthesia induction with 4% isoflurane, the lungs were lavaged with 0.5 mL of cooled saline via a tracheal catheter. The collected fluid was pooled into a single test tube.

2.6. Cell culture and treatment

The mouse lung epithelial cell line MLE-12 was purchased from Bena Culture Collection (Beijing, China). As an H_2S donor, sodium hydrosulfide (NaHS, S106641, Aladdin, Shanghai, China; purity: > 68%) was dissolved in sterile phosphate-buffered saline (PBS) to prepare a stock solution with a concentration of 100 mmol/L. Cells were exposed to NaHS (0, 0.1, 0.2, or 0.4 mM) in serum-free medium for 24 h. To prevent the escape of H_2S and maintain a stable exposure, the culture dishes were sealed with parafilm for 30 min and then removed. The cells were placed in a separate incubator to avoid affecting other cells, and collected at designated time points, with timing starting from the moment the cells were exposed to NaHS.

MLE-12 cells were transfected with 40 nM of either ATG10 siRNA or negative control NC siRNA (Sangon Biotech, China) using Lipofectamine 2000 reagent (Invitrogen, USA), followed by a 4–6-hour incubation in serum-free medium. Subsequently, the cells were exposed to treatment solutions containing 0 or 0.4 mM NaHS. Detailed information for the primers is in Table S2.

Mouse type II alveolar epithelial cells (mAEC-II) (Procell Life Science & Technology Co., Ltd., Wuhan) were cultured in medium specific for these cells (Procell Life Science & Technology Co., Ltd., Wuhan) at 37 °C in a humidified 5% CO_2 incubator. Surfactant Protein C (SP-C) is the most commonly used marker for mAEC-II [28]. We used immunofluorescence to identify mAEC-II and found that they expressed SP-C (Fig. S4).

2.7. Statistical analyses

Data are presented as means ± SD from at least three independent experiments. Statistical analyses were performed using GraphPad Prism 8.0 (GraphPad Software, USA). For comparisons between two groups, Student's *t*-test was used. For multiple group comparisons, one-way ANOVA followed by Tukey's *post hoc* test was applied. Correlation analyses were conducted using Pearson's correlation coefficient. Statistical significance was set at $^{*}P < 0.05$ or $^{**}P < 0.01$.

2.8. Other methods

Other methods are outlined in detail in the supplementary materials.

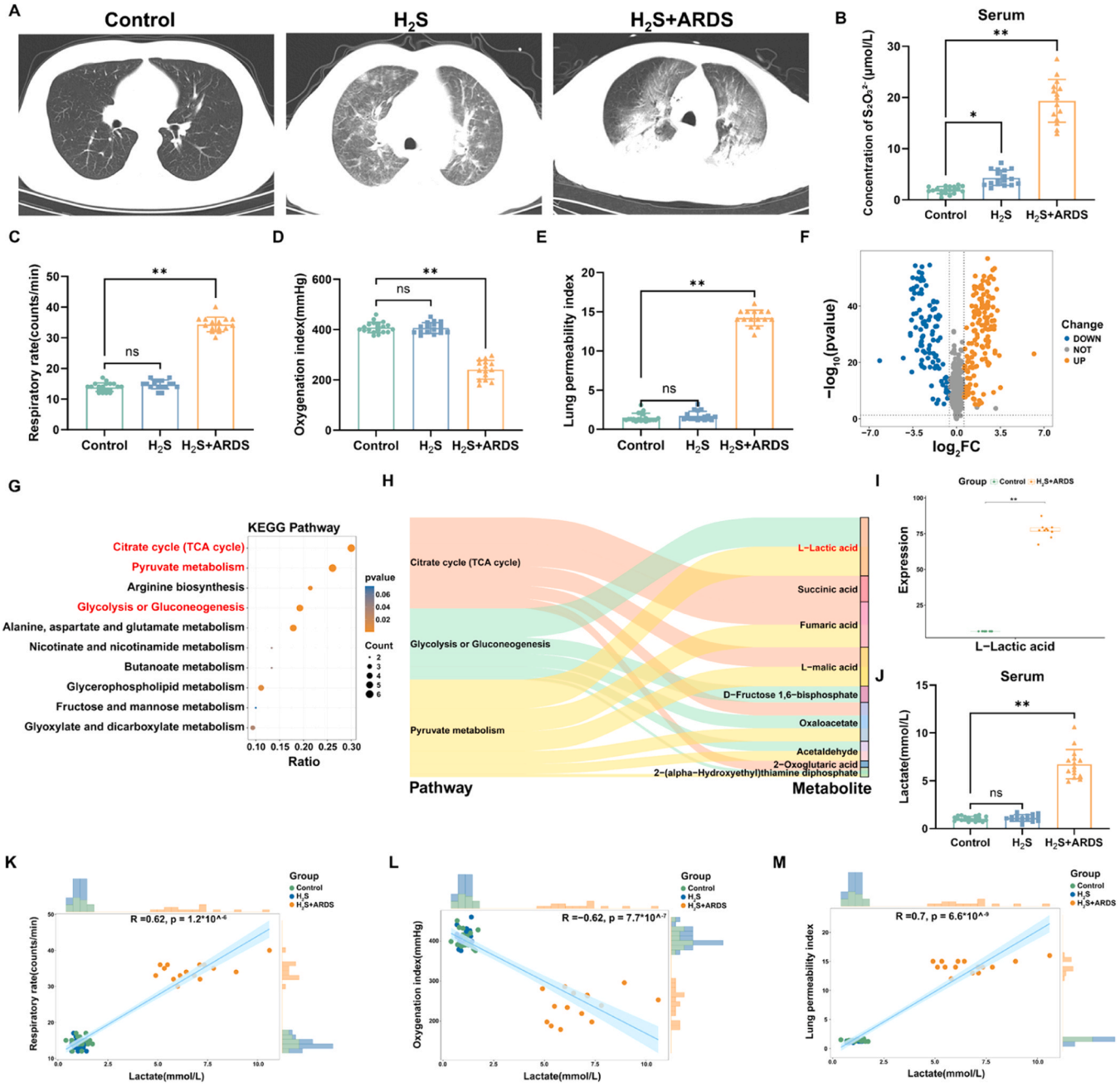

Fig. 1. Acute H_2S exposure causes increases of glycolysis and lactate levels in the serum of control humans and those with ARDS. Serum and BALF samples were collected from control (n = 20), H_2S (n = 17), and H_2S-induced ARDS humans (n = 15). (A) Typical CT imaging findings for control patients, those exposed to H_2S, and those with ARDS caused by H_2S inhalation. (B) The concentrations of $S_2O_3^{2-}$ in serum from these patients. (C) Respiratory rate, (D) oxygenation index, and (E) lung permeability index for the population. (F) Volcano plot of the identified metabolites. (G) Enrichment analysis for differentially expressed metabolites using MetaboAnalyst 5.0. (H) Sankey plot allowing visualization of the flow of differential metabolites across metabolic pathways. (I) Metabolomics-based relative abundance of L-lactic acid in serum among controls and patients with H_2S-induced ARDS (n = 10). (J) Serum lactate levels in the population. Correlation analyses between lactate levels and respiratory rates (K), oxygenation indices (L), and lung permeability indices (M). Data are presented as means ± SD; ns, no significance, *P < 0.05, ** P<0.01.

3. Results

3.1. Acute H_2S exposure causes increases of glycolysis and lactate levels in the serum and in the development of ARDS

Initially, we analyzed clinical indicators and chest CT manifestations of individuals from three groups: control, individuals exposed to H_2S who did not develop ARDS, and individuals with H_2S-induced ARDS. Upon reviewing the chest CT images, we observed that the control group exhibited clear lung markings with no abnormalities in lung field transparency. Lungs of the H_2S-exposed non-ARDS group showed slightly higher density patchy and linear shadows. In contrast, the H_2S-induced ARDS group displayed diffuse patchy dense shadows in lungs, with a characteristic butterfly wing appearance (Fig. 1A). Elevated serum thiosulfate ($S_2O_3^{2-}$), an H_2S metabolite, was also detected in exposed individuals relative to control, consistent with systemic H_2S exposure (Fig. 1B). The ARDS group demonstrated impaired respiratory function relative to controls, with a higher respiratory rate, a lower oxygenation index, and a higher lung permeability index. The H_2S-exposed non-ARDS group showed no such differences in these parameters (Fig. 1C-E). These results suggest that acute exposure to H_2S causes ARDS.

Metabolomics analysis revealed alterations in the serum metabolic profiles of the H_2S-induced ARDS group compared to controls (Fig. S1A and B). Screening for differential metabolites (VIP > 1, $P < 0.05$, and $|\log_2 FC| \geq 1$) identified 220 candidates (Fig. 1F). Subsequent Kyoto Encyclopedia of Genes and Genomes (KEGG) analysis implicated the pyruvate and glycolysis pathways as being centrally disrupted in H_2S-induced ARDS (Fig. 1G). Pathways were screened using thresholds of an impact value > 0.1 and a P value < 0.05 for further investigation. Among these, pathways related to L-lactate metabolism exhibited the most pronounced alterations (Fig. 1H). The metabolomics results showed that, compared with the control group, lactate levels in the H_2S-induced ARDS group were increased (Fig. 1I). Subsequently, we

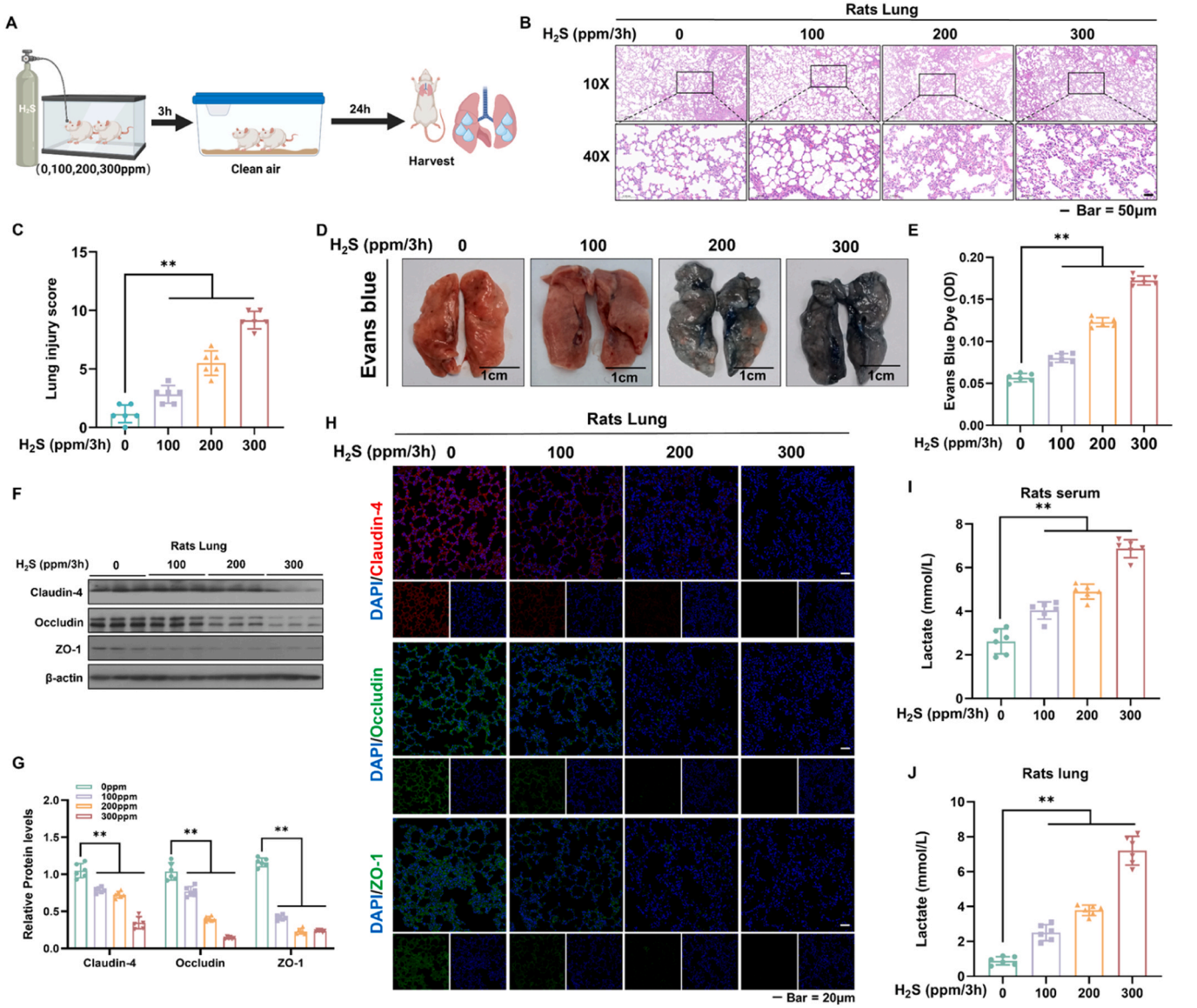

Fig. 2. Acute H_2S exposure induces ARDS coupled with rising lactate in rat serum and lung tissues. SD rats ($n = 6$) were exposed to 0, 100, 200 or 300 ppm H_2S in an acrylic container for 3 h, then moved to a normal air environment; lung tissues were taken under anesthesia after 24 h. (A) Diagram of acute H_2S exposure of rats. (B) Representative pictures of H&E staining. (C) Lung injury scores. (D) EB tracer in whole lungs of rats. (E) Quantification of EB dye contents. (F) Western blots for expression of Claudin-4, Occludin, and ZO-1 in lung tissues of rats. (G) Quantification of Western blots. (H) Expression of Claudin-4, Occludin, and ZO-1 in lung tissue of rats as determined by immunofluorescence assays (scale bar = 20 μm). (I) Lactate levels in rat serum. (J) Lactate levels in rat lungs. Data are presented as means ± SD; $^{**}P < 0.01$.

measured the lactate levels in serum. The results showed elevated levels in the H_2S-induced ARDS group (Fig. 1J). Lactate levels positively correlated with respiratory rate and lung permeability levels, and negatively correlated with the oxygenation index (Fig. 1K-M). These results identify lactate accumulation as a key metabolic event in H_2S exposure that underlies alterations in ARDS biomarkers.

3.2. Acute H_2S exposure induces ARDS coupled with rising levels of lactate in rat serum and lung tissues

By exposing SD rats to 0, 100, 200, or 300 ppm H_2S for 3 h, we established a rat model of ARDS induced by acute H_2S exposure. After exposure, the rats were transferred to a normal air environment, and

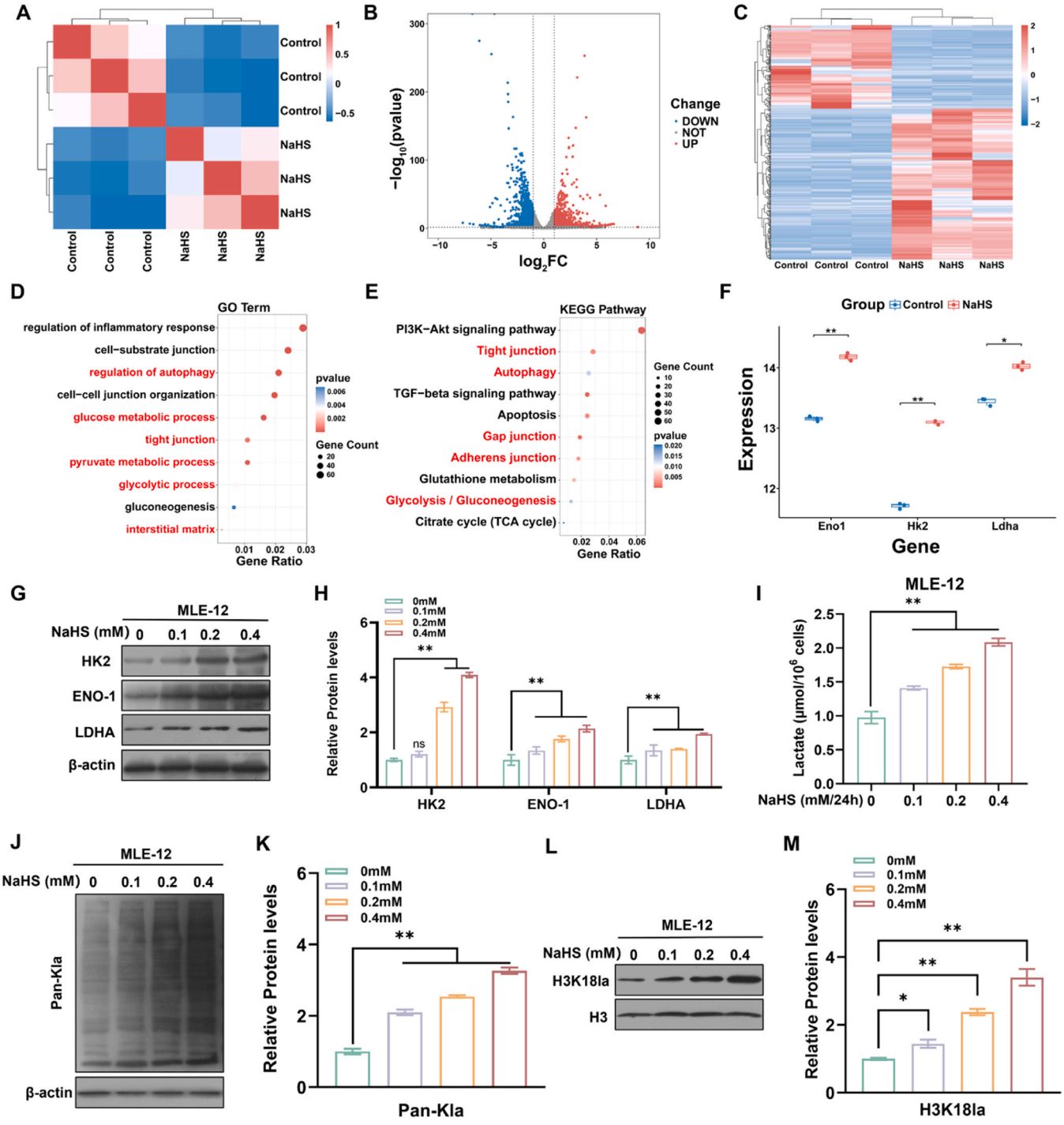

Fig. 3. NaHS induces increases of glycolysis and H3K18la in MLE-12 cells. MLE-12 cells were exposed to 0 or 0.4 mM NaHS for 24 h. (A) Heatmap of inter-sample correlation. (B) Volcano plot depicting the differentially expressed mRNAs between the NaHS-exposed MLE-12 groups and control groups. (C) Heatmap of differentially expressed mRNAs. (D) GO enrichment analysis of significantly dysregulated genes. (E) KEGG enrichment analysis of significantly dysregulated genes. (F) Differential expression of the *Eno-1*, *Hk2*, and *Ldha* genes in NaHS-treated MLE-12 cells compared with untreated MLE-12 cells. MLE-12 cells were exposed to 0, 0.1, 0.2, or 0.4 mM NaHS for 24 h. (G) Representative Western blots of HK2, ENO-1, and LDHA in MLE-12 cells. (H) Quantification of Western blots. (I) Lactate levels in NaHS-treated and untreated MLE-12 cells. (J) Representative Western blots of Pan-Kla in MLE-12 cells. (K) Quantitation of Western blots. (L) Representative Western blots of H3K18la in MLE-12 cells. (M) Quantitation of Western blots. Data are presented as means ± SD (n = 3); ns, no significance; $^*P < 0.05$; $^{**}P < 0.01$.

their lung tissues were collected 24 h later (Fig. 2A). H&E-stained sections revealed histopathological alterations in the lungs of exposed rats, featuring enhanced inflammatory cell infiltration; consolidation of alveolar spaces; destruction of alveolar walls; and dilated, congested pulmonary capillaries alongside alveolar hemorrhages and widened interstitial spaces (Fig. 2B). The lung injury scores increased with increases in H_2S exposure (Fig. 2C). For lung tissues, the results of staining with EB dye showed a higher EB content in H_2S-treated rats compared with the control group (Fig. 2D and E), suggesting increased permeability of the pulmonary barrier. H_2S exposure induced a series of pathophysiological alterations: a rise in serum thiosulfate ($S_2O_3^{2-}$, Fig. S2A), a decline in the arterial oxygenation index (Fig. S2B), and an increase in the lung wet/dry (W/D) ratio (Fig. S2C) and the lung permeability index (Fig. S2D), demonstrating impaired oxygenation and elevated lung permeability. We further observed that the expression levels of pulmonary epithelial barrier proteins, Claudin-4, Occludin, and ZO-1, were lower in the lung tissues of H_2S-exposed rats compared to the control group (Fig. 2F and G); this finding was validated via immunofluorescence tests (Fig. 2H), indicating disruption of the pulmonary epithelial barrier by H_2S. Lactate levels in the serum and lung tissues of H_2S-exposed rats were elevated compared to controls, showing a dose-dependent increase (Fig. 2I, J). Thus, for rats, acute exposure to H_2S increases lactate levels and leads to ARDS.

3.3. NaHS induces increases of glycolysis and H3K18la in alveolar epithelial cells

Treatment of MLE-12 cells with NaHS (0, 0.1, 0.2, 0.4 mM) for 24 h dose-dependently reduced the expression of the barrier proteins Claudin-4, Occludin, and ZO-1, as determined by Western blots (Fig. S3A, B). This effect was confirmed by immunofluorescence assays (Fig. S3C). The permeability of MLE-12 cells, as assessed by sodium fluorescein permeability assays and transepithelial electrical resistance (TEER) increased with increasing concentrations of NaHS (Fig. S3D and E). Consistent with the results obtained with MLE-12 cells, NaHS treatment downregulated the expression of barrier proteins (Fig. S4, Fig. S5A and B) and increased the permeability (Fig. S5C and D) of mAEC-II cells. These results indicate that NaHS increases the permeability of alveolar epithelial cells.

RNA sequencing of control and 0.4 mM NaHS-treated MLE-12 cells (Fig. 3A) identified 2675 differentially expressed genes, comprising 1381 upregulated and 1294 downregulated genes (Fig. 3B, C). Gene Ontology (GO) analysis indicated potential alterations in autophagy-related processes, tight junctions, pyruvate metabolism, and glycolysis (Fig. 3D). KEGG pathway analysis showed significant changes in tight junctions, autophagy, adherens junctions, and glycolysis pathways (Fig. 3E). The transcriptomic results revealed that, in NaHS-treated MLE-12 cells, the mRNA levels of glycolytic enzymes *Eno-1*, *Hk2*, and *Ldha* were elevated compared to the control group (Fig. 3F). Western blots showed that, for MLE-12 cells, NaHS treatment upregulated the expression of glycolytic enzymes HK2, ENO-1 and LDHA (Fig. 3G and H), an effect that was concomitant with increases in intracellular lactate content (Fig. 3I). Consistent with the results obtained in MLE-12 cells, NaHS treatment upregulated the expression of glycolytic enzymes (Fig. S6A and B) and lactate levels (Fig. S6C) in mAEC-II cells. These results show that, for alveolar epithelial cells, NaHS induces increases of glycolysis and lactate.

In a rat model of H_2S-induced ARDS, acute H_2S exposure upregulated protein expressions of the glycolytic enzymes HK2, ENO-1, and LDHA in lung tissues (Fig. S7A, B) and concomitantly increased lactate levels (Fig. S7C). Western blots demonstrated that acute H_2S exposure increased the Pan-Kla levels in lung tissues (Fig. S8A and B). We subsequently examined the lactylation levels at various histone sites and found that H3K18la expression was elevated, but changes in lactylation levels at other sites such as H3K9, H3K14, H4K8, and H4K12 were not statistically significant (Fig. S8C and D). The change in H3K18la expression exhibited a dose-response relationship (Fig. S8E and F). Western blots revealed that NaHS treatment increased Pan-Kla (Fig. 3J and K) and H3K18la levels (Fig. 3L and M) in MLE-12 cells in a dose-dependent manner. Consistent with the results for MLE-12 cells, NaHS treatment upregulated the Pan-Kla (Fig. S9A and B) and H3K18la levels (Fig. S9C and D) in mAEC-II cells, with a general dose-response relationship. These findings demonstrate that H_2S promotes glycolysis and increases H3K18la levels.

3.4. Identification of downstream target genes of H3K18la in NaHS-treated MLE-12 cells

Subsequently, we employed cleavage under the targets and tagmentation (CUT&Tag) technology to screen for downstream regulatory genes of H3K18la under NaHS treatment (Fig. 4A). NaHS induced the enrichment of H3K18la in gene promoter regions (Fig. 4B-D). GO analysis revealed enrichment in autophagy processes (Fig. 4E), and KEGG pathway analysis showed significant changes in the autophagy pathway (Fig. 4F). By integrating two analyses containing two datasets, we identified 454 genes, among which 77 genes exhibited significant expression in NaHS-induced H3K18la upregulation, including ATG10, which is involved in the autophagy pathway (Fig. S10A and Fig. 4G). The results of qRT-PCR indicated that NaHS treatment led to an increase in the mRNA levels of *Atg10*, with a dose-effect relationship (Fig. S10B). Notably, NaHS treatment led to the enrichment of H3K18la in the ATG10 promoter region (Fig. 4H), a phenomenon that was verified by Chromatin Immunoprecipitation (ChIP) assays (Fig. 4I). Our findings demonstrate that NaHS-induced, ATG10-mediated autophagy in MLE-12 cells is mechanistically linked to H3K18la.

3.5. ATG10 is involved in NaHS-induced increases of autophagy and cell permeability of alveolar epithelial cells

Subsequently, we validated the NaHS-induced changes in ATG10 and autophagy levels through *in vitro* experiments and explored the relationship between these factors. Western blots showed that, for MLE-12 cells, NaHS treatment enhanced the expression of ATG10 and the LC3-II/I ratio, with a concomitant reduction in P62 (Fig. 5A and B). Immunofluorescence results confirmed the changes in ATG10 (Fig. 5C). Transmission electron microscopy (TEM) and GFP-LC3 fluorescence showed an increase in autophagosomes following NaHS treatment (Fig. 5D). Consistent with the results obtained with MLE-12 cells, NaHS treatment upregulated the autophagy levels in mAEC-II cells, with a general dose-response relationship (Fig. S11A-C). These findings demonstrate, for alveolar epithelial cells, a dose-dependent induction of autophagy following NaHS treatment. Similarly, in our rat model of H_2S-induced ARDS, we noted consistent changes: acute hydrogen sulfide exposure resulted in an increase in autophagic activity in the lung tissues of rats (Fig. S12A-C).

Subsequently, MLE-12 cells were treated with ATG10 siRNA prior to NaHS treatment (Fig. S13A and B). Reversal of the NaHS-mediated increase in LC3-II/I and the decrease in P62 by ATG10 siRNA confirmed a leading role for ATG10 in this process, as evidenced by Western blots (Fig. 5E and F). TEM revealed that knockdown of ATG10 alleviated the increase in autophagosomes induced by NaHS (Fig. S13C). The GFP-LC3 fluorescence results validated the changes in autophagosomes (Fig. S13C). Knockdown of ATG10 also mitigated the decrease in barrier protein expression induced by NaHS (Fig. 5G and H), a result confirmed by immunofluorescence assays (Fig. 5I). Permeability assays of MLE-12 cells showed that knockdown of ATG10 alleviated the increase in permeability induced by NaHS (Fig. 5J and K). Thus, in MLE-12 cells, ATG10 is involved in NaHS-induced autophagy overactivation and barrier dysfunction.

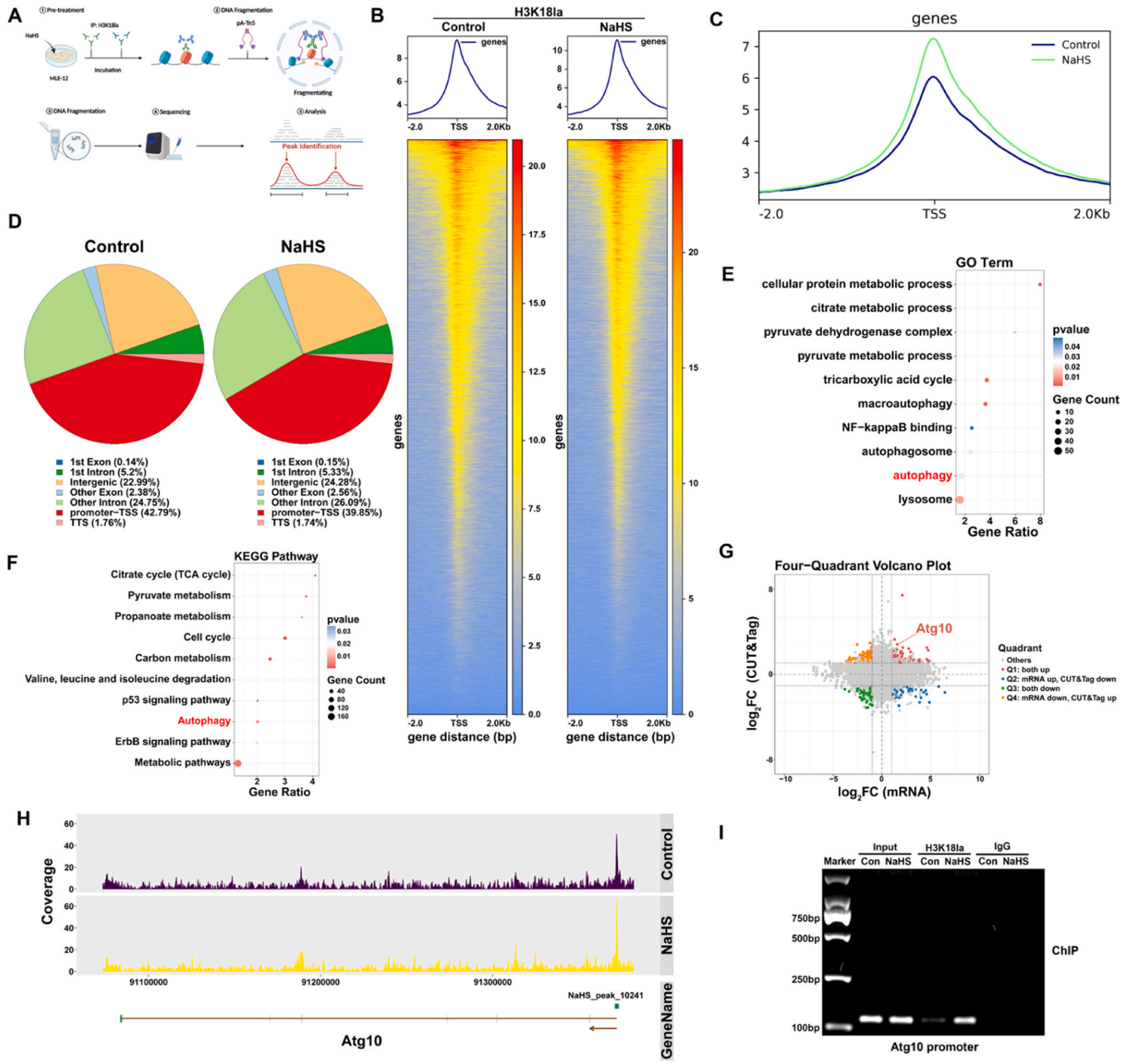

Fig. 4. Identification of downstream target genes of H3K18la in NaHS-treated MLE-12 cells. (A) Schematic illustration of the CUT&Tag process. (B) Heatmap showing the binding peak positions and signal intensities of H3K18la for all genes in the genome. (C) Distribution of reads near the transcription start sites (TSS). (D) Pie chart showing the genome-wide distribution of H3K18la binding peaks. (E) The GO enrichment of significantly dysregulated genes. (F) The KEGG enrichment analysis of significantly dysregulated genes. (G) Quadrant plot of differentially expressed genes from the joint analysis of CUT&Tag and transcriptome. (H) Integrative Genomics Viewertracks for ATG10 from H3K18la CUT&Tag analysis. (I) The level of H3K18la in the ATG10 promoter region of MLE-12 cells as determined by ChIP-RT-PCR.

3.6. DCA, via inhibiting glycolysis, alleviates the increases of autophagy and permeability in MLE-12 cells induced by NaHS

To determine whether NaHS-driven glycolysis was responsible for the observed effects, MLE-12 cells were treated with the glycolytic inhibitor DCA. This intervention abolished the NaHS-induced upregulation of key glycolytic enzymes (Fig. S14A and B). In these cells, DCA also inhibited the NaHS-induced elevations in lactate levels (Fig. 6A), Pan-Kla (Fig. 6B and C), and H3K18la (Fig. 6D and E). Compared with cells exposed to NaHS, the level of H3K18la in the ATG10 promoter region was reduced in cells treated with DCA (Fig. 6F). In addition, DCA blocked the increase in autophagy levels and the decrease in barrier protein expression induced by NaHS (Fig. 6G and H). Immunofluorescence results confirmed that DCA blocked the increase in ATG10 expression induced by NaHS (Fig. 6I) and the decrease in barrier protein expression caused by NaHS (Fig. S14C). Consistent with this, TEM and GFP-LC3 fluorescence system results showed that DCA inhibited the increase in autophagosomes in MLE-12 cells treated with NaHS (Fig. 6J). Moreover, DCA inhibited the increase in permeability of MLE-12 cells caused by NaHS (Fig. 6K and L). These results demonstrate that NaHS promotes autophagy and increases permeability of MLE-12 cells, effects that are abolished by the glycolytic inhibitor DCA.

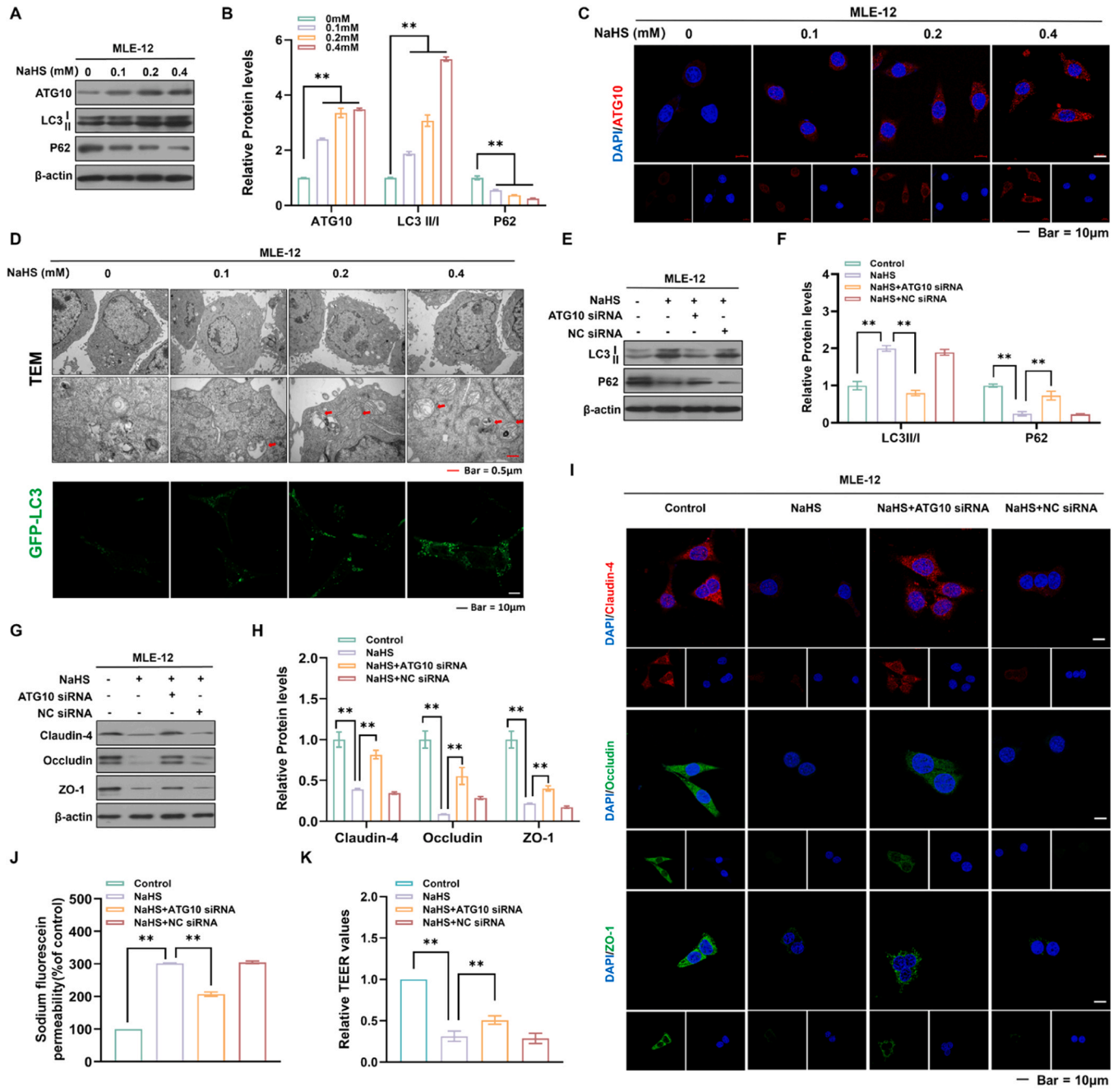

Fig. 5. ATG10 is involved in NaHS-induced increases of autophagy and cell permeability in MLE-12 cells. MLE-12 cells were exposed to 0, 0.1, 0.2, or 0.4 mM NaHS for 24 h. (A) Representative Western blots of ATG10, LC3, and P62 in MLE-12 cells. (B) Quantification of Western blots. (C) Representative immunofluorescence images of ATG10 in MLE-12 cells (scale bar = 10 μm). (D) Ultrastructural changes of autophagosomes (red arrows) in MLE-12 cells observed by TEM (scale bar = 0.5 μm) and representative images for GFP-LC3 (green) (scale bar = 10 μm). MLE-12 cells transfected with ATG10 siRNA or NC siRNA were treated with 0 or 0.4 mM NaHS for 24 h. (E) Representative Western blots of LC3 and P62 in MLE-12 cells. (F) Quantification of Western blots. MLE-12 cells were transfected with ATG10 siRNA or NC siRNA and then exposed to 0 or 0.4 mM NaHS for 24 h. (G) Representative Western blots of Claudin-4, Occludin, and ZO-1 in MLE-12 cells. (H) Quantification of Western blots. (I) Immunofluorescence staining of Claudin-4, Occludin, and ZO-1 in MLE-12 cells (scale bar =10 μm). (J) The sodium fluorescein permeability experiment. (K) The TEER experiment. Data are presented as means ± SD (n = 3); ns, no significance; *P < 0.05; **P < 0.01.

3.7. H3K18la is involved in NaHS-increased permeability of MLE-12 cells by activating ATG10-mediated autophagy

The functions of H3K18la and ATG10 were further assessed in a rescue experiment in which ATG10 was overexpressed in the context of DCA-inhibited lactate production. DCA blocked the NaHS-induced increase of ATG10 and LC3 II/I levels, which were reversed by the overexpression of ATG10. DCA blocked the NaHS-caused decrease of P62 and levels of barrier proteins (Claudin-4, Occludin, and ZO-1), which were reversed by the overexpression of ATG10 (Fig. 7A and B). The changes of ATG10 (Fig. 7C) and barrier proteins (Fig. S15) were confirmed by immunofluorescence results. Consistent with this model, TEM and GFP-LC3 fluorescence results showed that the suppression of NaHS-induced autophagy by DCA in MLE-12 cells was rescued by ATG10 overexpression (Fig. 7C). Finally, the suppressive effect of DCA on NaHS-induced hyperpermeability was reversed by ATG10 overexpression (Fig. 7D and E). These results demonstrate that, in MLE-12 cells, H3K18la drives increased cellular permeability by activating

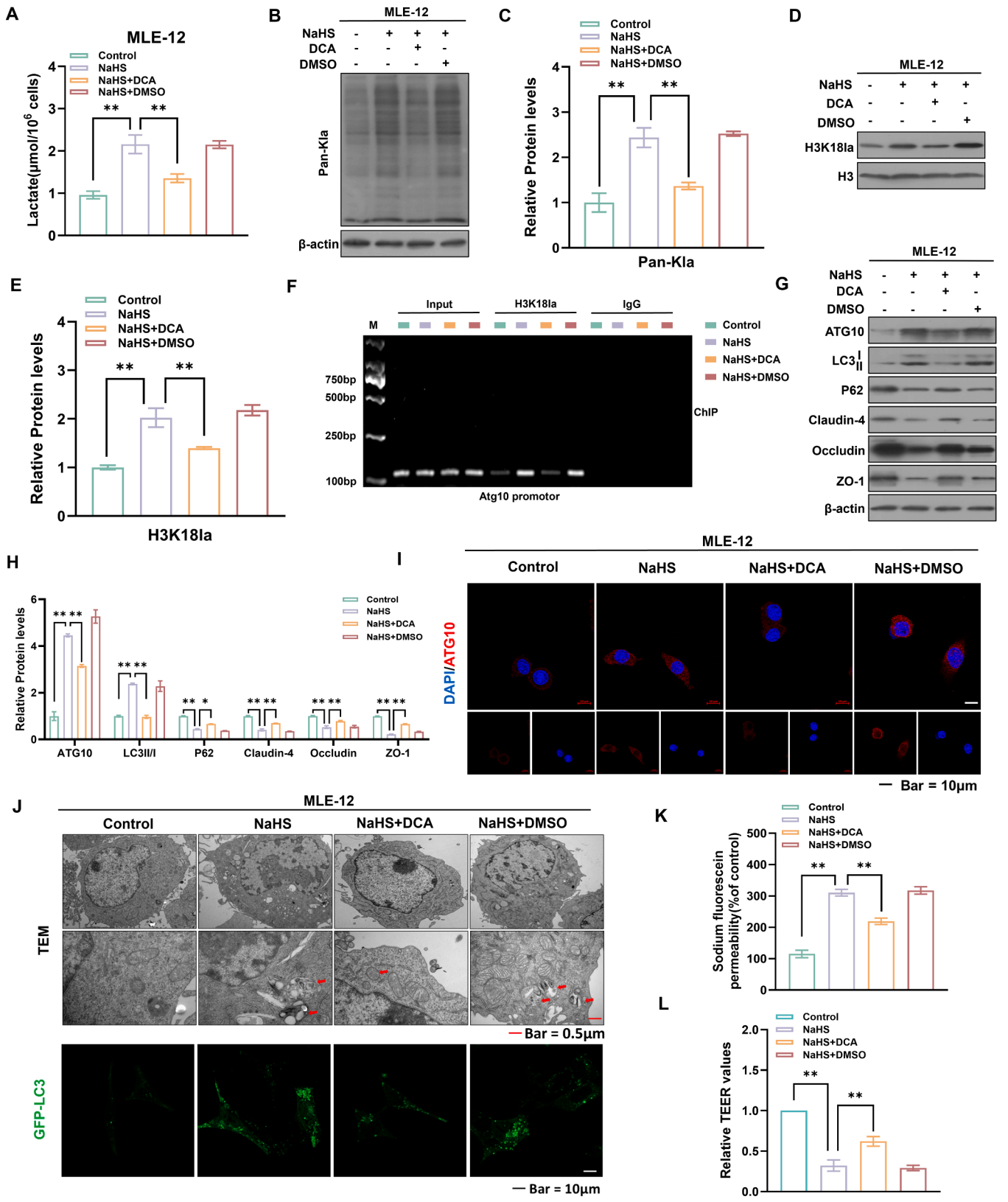

Fig. 6. DCA, via inhibiting glycolysis, alleviates the increases of autophagy and permeability induced by NaHS in MLE-12 cells. MLE-12 cells were exposed to 0 or 0.4 mM NaHS or to 0.4 mM NaHS combined with 10 mM DCA for 24 h. (A) Lactate levels in MLE-12 cells. (B) Representative Western blots of Pan-Kla in MLE-12 cells. (C) Quantification of Western blots. (D) Representative Western blots of H3K18la in MLE-12 cells. (E) Quantification of Western blots. (F) Levels of H3K18la at the ATG10 promoter in MLE-12 cells as determined by ChIP-RT-PCR. (G) Representative Western blots of ATG10, LC3, P62, Claudin-4, Occludin, and ZO-1 in MLE-12 cells. (H) Quantification of Western blots. (I) representative immunofluorescence images of ATG10 in MLE-12 cells (scale bar = 10μm). (J) Ultrastructural changes of autophagosomes (red arrows) in MLE-12 cells as observed by TEM (scale bar = 0.5 μm) and representative images of GFP-LC3 (green) (scale bar = 10 μm). (K) The sodium fluorescein permeability experiment. (L) The TEER experiment. Data are presented as the means ± SD (n = 3); *$P < 0.05$; **$P < 0.01$.

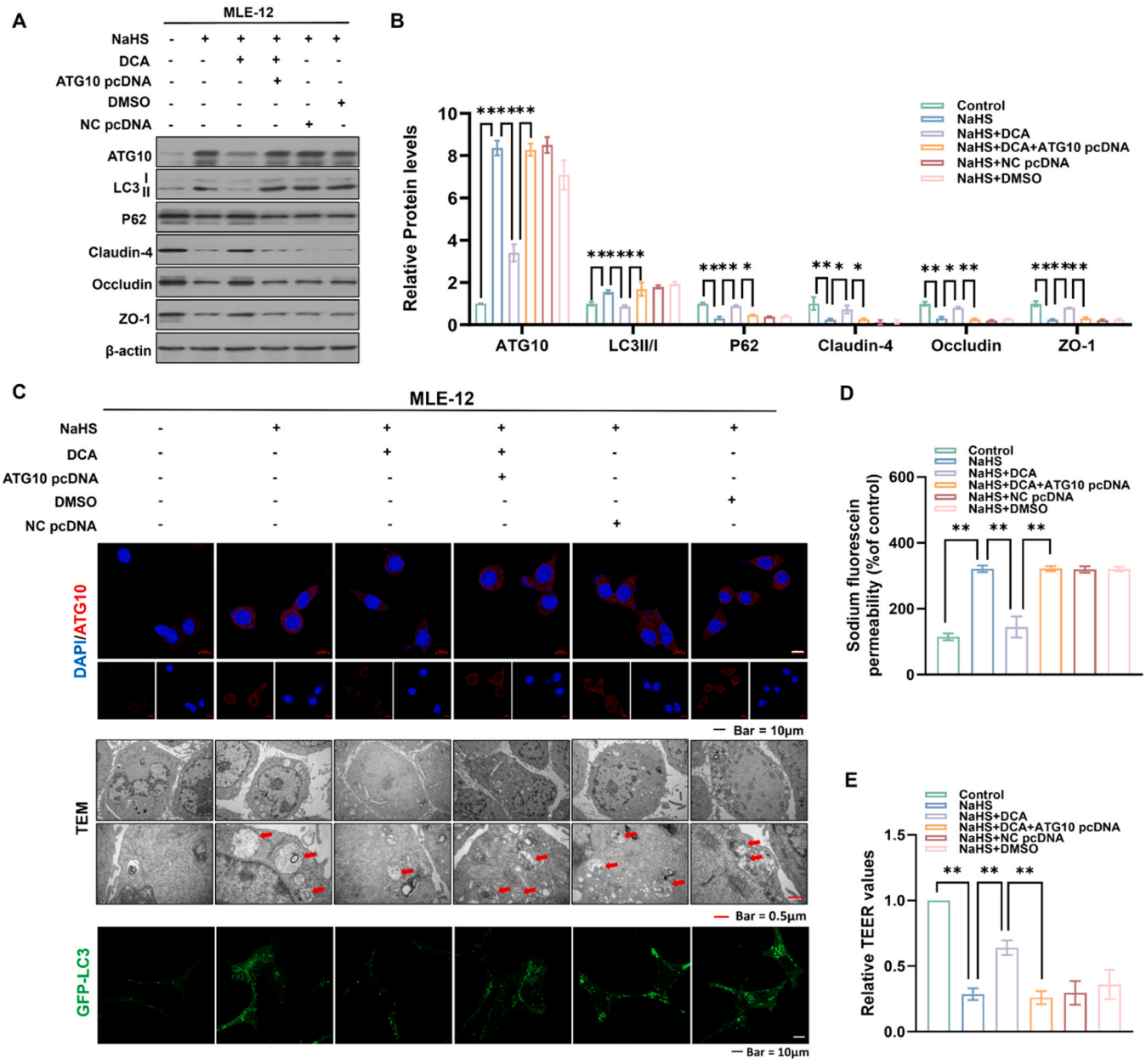

Fig. 7. H3K18la is involved in NaHS-induced increased permeability of MLE-12 cells by activating ATG10-mediated autophagy. MLE-12 cells were exposed to 10 mM DCA or to 10 mM DCA and then transfected with ATG10 pcDNA for 24 h and then exposed to 0 or 0.4 mM NaHS for 24 h. (A) Representative Western blots of ATG10, LC3, P62, Claudin-4, Occludin, and ZO-1 in MLE-12 cells. (B) Quantification of Western blots. (C) Representative immunofluorescence images of ATG10 in MLE-12 cells (scale bar = 10 μm); ultrastructural changes of autophagosomes (red arrows) in MLE-12 cells as observed by TEM (scale bar = 0.5 μm) and representative images of GFP-LC3 (green) (scale bar = 10 μm). (D) The sodium fluorescein permeability experiment. (E) The TEER experiment. Data are presented as means ± SD (n = 3); $^{*}P < 0.05$; $^{**}P < 0.01$.

ATG10-mediated autophagy.

3.8. *DCA inhibits glycolysis, thereby blocking the increase in autophagy and the disruption of the lung epithelial barrier in H_2S-induced ARDS rats*

To evaluate the therapeutic potential of targeting H3K18la in H_2S-induced ARDS, we investigated the efficacy of DCA in alleviating lung injury in rats (Fig. S16A). DCA treatment suppressed the H_2S-induced upregulation of key glycolytic enzymes (Fig. S16B and C); it also reversed the increase in lactate levels in serum (Fig. S16D) and lung tissue induced by H_2S (Fig. 8A). DCA also inhibited the elevation of Pan-Kla (Fig. 8B and C) and H3K18la levels induced by H_2S (Fig. 8D and E). The results of Western blots indicated that DCA blocked the increase in autophagy and the decrease in barrier protein expression induced by NaHS (Fig. 8F and G); immunofluorescence assays confirmed the effect of DCA on barrier proteins induced by NaHS (Fig. S16E). TEM results showed that DCA partially reversed the increase in autophagosomes caused by H_2S exposure (Fig. 8H). H&E staining revealed that, for rats, DCA treatment ameliorated H_2S-induced lung injury, reducing characteristic pathological features, including inflammatory cell infiltration and alveolar hemorrhage (Fig. 8I), which corresponded to lower scores for lung injury (Fig. 8J). In addition, DCA alleviated the decrease in the arterial oxygenation index (Fig. S16F), the increase in lung permeability index (Fig. S16G), and the increase in lung tissue W/D ratios caused by H_2S exposure (Fig. 8K). Our findings demonstrate that, in rats, DCA attenuates the development of H_2S-induced ARDS by suppressing

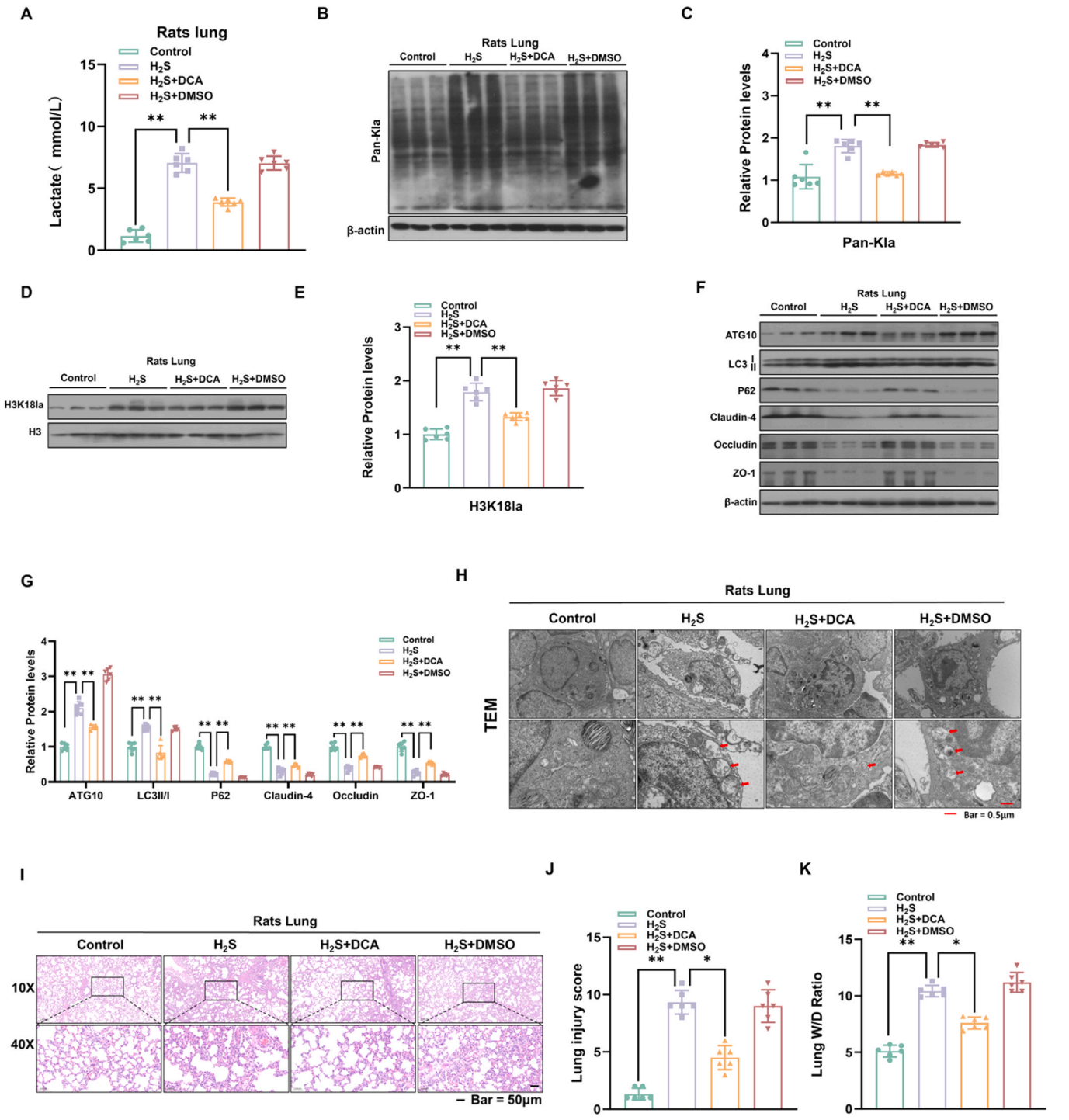

Fig. 8. DCA inhibits glycolysis, thereby blocking the increase in autophagy and disruption of the lung epithelial barrier in H_2S-induced ARDS rats. SD rats (n = 6) were exposed to 0 or 300 ppm H_2S in an acrylic container for 3 h. Subsequently, the H_2S-exposed rats were administered intraperitoneal injections of either 10 mg/kg DCA or DMSO. The rats were then transferred to a normal air environment. After 24 h, lung tissues were collected under anesthesia. (A) Lactate levels in rat lungs. (B) Representative Western blots of Pan-Kla in rat lungs. (C) Quantification of Western blots. (D) Representative Western blots of H3K18la in rat lungs. (E) Quantification of Western blots. (F) Representative Western blots of ATG10, LC3, P62, Claudin-4, Occludin, and ZO-1 in rat lungs. (G) Quantification of Western blots. (H) Ultrastructural changes of autophagosomes (red arrows) in rat lungs observed by TEM (scale bar = 0.5 μm). (I) Representative pictures of H&E staining. (J) Lung injury scores. (K) Lung W/D ratios for rats. Data are presented as means ± SDs; ns, no significance; *P <0.05; **P< 0.01.

glycolysis.

4. Discussion

H_2S poisoning is commonly associated with accidents and is a major cause of occupational fatalities in the industrial sector. In China, it ranks second among fatal incidents involving toxic gases. In the event of mass exposure, it can lead to serious public health emergencies, posing a substantial threat to human health [29]. Exposure of humans to H_2S is predominantly acute, occurring primarily via the respiratory tract. Prolonged inhalation of high concentrations of H_2S may successively trigger ALI and ARDS. ARDS is a respiratory disorder characterized by

hypoxemia, pulmonary edema, and reduced lung compliance, with a global mortality rate as high as 30–35% [30]. The pathogenesis of ARDS involves various mechanisms, primarily including disruption of the alveolar-capillary barrier, cell death and dysfunction, and the activation of pro-inflammatory signals [31]. Therefore, elucidating its molecular mechanisms is relevant for identifying potential therapeutic targets. This study reveals the mechanism by which acute H_2S poisoning induces enhanced glycolysis and lactate accumulation in pulmonary epithelial cells, subsequently activating ATG10-mediated excessive autophagy, which disrupts the pulmonary epithelial barrier and leads to ARDS. The findings elucidate the close association between metabolic reprogramming and disruption of the pulmonary epithelial barrier. Specifically, during ARDS, alveolar epithelial cells exhibit enhanced glycolysis, leading to lactate accumulation, which through H3K18la-mediated activation of ATG10 transcription, triggers excessive autophagy in alveolar epithelial cells and subsequent disruption of the pulmonary epithelial barrier. Targeted regulation of glycolysis in alveolar epithelial cells reduces lactic acid production and autophagy, providing a strategy for alleviating H_2S-induced ARDS.

Alveolar epithelial cells serve, on the one hand, to form a natural physical barrier against exogenous microorganisms and fine particulate matter, and, on the other hand, to activate various immune cells to initiate the innate immune response. When the integrity of the epithelial barrier is compromised, inflammatory cells, protein exudates, and hyaline membranes enter the alveolar space, leading to pulmonary edema, impaired gas exchange, and refractory hypoxemia [32]. In sepsis-induced ALI, elevated HDAC3 deacetylates FOXO1 and promotes RCOK1 transcription; elevated RCOK1 facilitates mitochondrial fission and mitochondrial autophagy, as well as reducing fatty acid oxidation, thereby disrupting the epithelial barrier [33]. In a mouse model of LPS-induced ARDS, elevated ROS promotes the phosphorylation of DRP1 at Ser616, thereby facilitating mitochondrial fission, causing damage to epithelial tight junctions and inducing apoptosis, ultimately compromising the integrity of the epithelial barrier [7]. Furthermore, H_2S exposure induces oxidative stress and the release of inflammatory cytokines, leading to the loss of tight junction proteins and epithelial barrier dysfunction, thereby increasing the susceptibility of the lungs to pathogen invasion [34]. This indicates that the alveolar epithelial barrier is involved in maintaining alveolar structural stability, defending against pathogen invasion and regulating pulmonary immune responses; its integrity is necessary for maintaining normal gas exchange and preventing the onset of ALI. Our results demonstrate that acute H_2S exposure induces ARDS in rats, manifested by increased respiratory rate, decreased arterial oxygenation index, and elevated lung injury scores, accompanied by downregulation of barrier proteins such as Claudin-4, Occludin, and ZO-1 as well as increased cellular permeability. Thus, disruption of the pulmonary epithelial barrier is a key pathological step in the pathogenesis of H_2S-induced ARDS.

The role of metabolic reprogramming in ARDS is now recognized. As the end product of glycolysis, lactate is generated from pyruvate under the catalysis of lactate dehydrogenase, and its accumulation typically reflects an increase in cellular glycolytic metabolic activity [35]. Enhanced glycolysis is regulated by several rate-limiting enzymes, including HK2, ENO-1. and LDHA [36]. In Down syndrome, excessive activation of the CBS/H_2S pathway inhibits oxidative phosphorylation and induces compensatory enhancement of glycolysis, suggesting that H_2S has the capacity to drive metabolic reprogramming [37]. Consistent with this, we observed that acute H_2S exposure induced lactate accumulation across human, cellular, and animal models. In clinical samples, we found elevated lactate levels in patients with H_2S induced ARDS, and correlation analysis indicated that elevated serum lactate levels were associated with respiratory rate, oxygenation index, and indicators of lung permeability. Furthermore, in NaHS-treated MLE-12 cells, RNA-seq results showed significant enrichment of the glycolysis and pyruvate metabolism pathways, and both protein and mRNA levels of HK2, ENO-1, and LDHA were elevated, accompanied by lactate accumulation. Furthermore, in lung tissue from rats exposed to acute H_2S, levels of HK2, ENO-1, and LDHA were elevated, and lactate accumulated. This indicates that the elevation in lactate levels caused by acute H_2S-induced ARDS is not a coincidental concomitant phenomenon, but rather a key feature of H_2S induced ARDS.

Lactylation is a lactate-mediated post-translational modification that regulates gene expression and cellular function by covalently attaching a lactate group to lysine residues on histones or other proteins [38]. Histone lactylation is a key mechanism underlying lactate-mediated disease progression [39]. In the tumor microenvironment, lactate upregulates the m6A methyltransferase METTL3 in tumor-infiltrating myeloid cells by inducing H3K18la, thereby enhancing the m6A modification and translation efficiency of JAK1 mRNA, and leading to STAT3 phosphorylation and the establishment of an immunosuppressive state [40]. In sepsis-induced ARDS, enhanced glycolysis leads to lactate accumulation and H3K14la, which in turn upregulates the transcription of ferrocytosis-related genes such as TFRC and SLC40A1, inducing ferroptosis and dysfunction in pulmonary endothelial cells, thereby exacerbating pulmonary vascular injury [41]. Exposure to cigarette smoke may also accelerate the progression of Alzheimer's disease by promoting NLRP3 transcription through the induction of H4K12la [36]. In our study, we found elevated levels of Pan-Kla and H3K18la in rat lung tissue following acute H_2S exposure and in NaHS-treated MLE-12 cells. Furthermore, CUT&Tag sequencing results indicated that NaHS induced the enrichment of H3K18la in the ATG10 promoter region, a finding validated by ChIP-RT-PCR experiments. Therefore, acute H_2S exposure may promote the activation of ATG10 transcription and upregulation of its expression by elevating H3K18la levels and enhancing its enrichment at the ATG10 promoter.

During autophagy, ATG10, an autophagy-associated E2-like enzyme, mediates the covalent binding of ATG12 and ATG5 to form the ATG12-ATG5 complex, thereby participating in the formation and extension of the autophagosome membrane; ATG10 is a regulatory factor in the autophagy process [42]. In neuronal models with TBK1 mutations, ATG10-dependent autophagy abnormalities are accompanied by the accumulation of SQSTM1/P62, suggesting that ATG10 has a function in maintaining autophagy homeostasis [43]. The lncRNA SNHG1 suppresses ATG10-mediated excessive autophagy by stabilizing *Bhlhe40* mRNA and promoting PIAS3-mediated SUMOylation and nuclear translocation of the Bhlhe40 protein, thereby alleviating high-glucose-induced calcification and senescence in vascular smooth muscle cells [44]. These findings indicate that ATG10 upregulation drives autophagy activation and contributes to the development of various disease phenotypes. Consistent with previous studies, we found that, following NaHS treatment of MLE-12 cells, ATG10 levels were elevated, accompanied by an increase in the LC3-II/I ratio, a decrease in P62, and an increase in autophagosomes observed under TEM, suggesting an enhancement in autophagy levels. Upon ATG10 knockdown, the NaHS-induced increase in LC3-II/I and decrease in P62 were reversed; the number of autophagosomes decreased; the levels of Claudin-4, Occludin, and ZO-1 recovered; and cell permeability decreased. These results indicate that changes in ATG10 levels represent a key link between histone lactylation and autophagy.

The role of autophagy in acute lung injury is bidirectional and phase-dependent; moderate autophagy exerts a protective effect by clearing damaged organelles and abnormal proteins, and alleviating oxidative stress and inflammatory responses [45]. Excessive activation of autophagy may disrupt protein homeostasis, leading to dysregulation of autophagy, epithelial cell dysfunction, and even cell death, and has a impact on chronic damage to the respiratory system and the disruption of tissue homeostasis [46,47]. In alveolar epithelial cells, *Streptococcus pneumoniae* induces BECN1 phosphorylation and activates autophagy by releasing extracellular vesicles containing the virulence protein StkP, thereby promoting autophagy-dependent Occludin degradation and disrupting function of the alveolar epithelial barrier [48]. In alveolar epithelial cells, LPS induces elevated RAGE levels in mouse lung tissue,

leading to activation of autophagy, which promotes apoptosis and ultimately disrupts the alveolar epithelial barrier [49]. These results indicate that excessive autophagy activation is associated with the disruption of the integrity of the alveolar epithelial barrier. We found that NaHS-induced autophagy enhancement is accompanied by a decrease in pulmonary epithelial barrier proteins and increased permeability; downregulation of ATG10 expression blocks the excessive autophagy activation and increased cellular permeability caused by NaHS treatment of MLE-12 cells and restores function of the pulmonary epithelial barrier.

Lactylation is involved in the regulation of autophagy, suggesting that lactate acts as a bridge linking glycolysis and autophagy via lactylation [50]. Its function is not limited to signaling a state of metabolic activity; rather, through histone lactylation or protein lactylation, it directly influences processes such as the transcription of autophagy-related genes, autophagosome maturation, and mitochondrial autophagy. In colorectal cancer, tumor-derived lactate upregulates the transcription of RUBCNL/Pacer via H3K18la, promoting autophagosome maturation and leading to bevacizumab resistance [51]. Following traumatic brain injury, histone lactylation upregulates PSMD14, which in turn activates PINK1-mediated mitophagy by deubiquitinating PKM2, thereby alleviating neuronal PANoptosis [52], supporting the functional role of lactylation in the regulation of autophagy. In glioblastoma, the H4K8la-NUPR1 axis mediates protective autophagy while promoting tumor progression [53]. Our results show that, in acute H_2S-induced pulmonary edema, lactylation is a key mechanism linking metabolic reprogramming to autophagy activation. We consistently observed enhanced glycolysis and lactate accumulation in human samples, an acute H_2S-exposed rat model, and NaHS-treated MLE-12 cells; in cellular and animal lung tissues, H3K18la was the most significantly elevated histone lactic acid modification site. CUT&Tag and ChIP results confirmed that NaHS promotes the enrichment of H3K18la in the ATG10 promoter region, accompanied by upregulation of ATG10 transcription; these findings indicate that H3K18la is not merely an epigenetic alteration occurring in tandem with elevated lactate levels, but rather, by promoting the transcriptional activation of ATG10, it enhances autophagy and mediates the disruption of the pulmonary epithelial barrier.

DCA, as a classic regulator of glycolysis, reduces lactate production, improves energy metabolism disorders, and alleviates tissue damage in various diseases associated with metabolic reprogramming [54]. For pediatric patients with lactic acidosis, DCA reduces blood lactate levels and stabilizes acid-base balance [55]. For diabetic nephropathy, DCA intervention reduces the binding between Glis1 and KAT5, thereby inhibiting histone H3 lactylation and suppressing the senescence of renal tubular epithelial cells, thus mitigating progression of the disease [56]. During the progression of MAFLD, lactic acid accumulation induces H4K16la, thereby activating PDK4 transcription and inhibiting the entry of pyruvate into mitochondrial oxidative metabolism, promoting glycolysis and lipid accumulation, and driving the development of hepatic steatosis, inflammation, and fibrosis; DCA alleviates these effects by intervening at the glycolytic level [57]. However, the therapeutic role of DCA in ARDS caused by acute H_2S exposure remains unclear. Our study applied DCA intervention at the cellular and animal levels, and the results demonstrated that DCA exerts an inhibitory effect on H_2S-induced lung injury.

5. Conclusion

In summary, through metabolomics and clinical indicator analysis of H_2S-exposed populations, studies with acute H_2S-exposed rats and DCA-intervened rats, as well as *in vitro* studies employing NaHS exposure combined with various cell treatment approaches, this work revealed that: acute H_2S exposure enhances glycolysis in alveolar epithelial cells, leading to lactate accumulation; the accumulated lactate induces H3K18la, thereby promoting ATG10 transcription, causing excessive autophagy activation in alveolar epithelial cells, consequently damaging the alveolar epithelial barrier, and resulting in development of ARDS. DCA partially alleviates these H_2S-induced pathological effects by inhibiting glycolysis, thereby blocking ARDS caused by acute exposure to H_2S. These findings elucidate molecular mechanisms underlying H_2S-induced ARDS and provide new evidence for identifying precise therapeutic targets and early molecular biomarkers for patients with H_2S-induced ARDS.

CRediT authorship contribution statement

Bingyu Ling: Conceptualization, Data curation, Methodology, Writing – original draft, Funding acquisition, Visualization. **Ping Geng:** Methodology, Data curation, Visualization. **Bowen Fan:** Methodology, Software, Visualization. **Xiaolong Wu:** Methodology, Validation. **Yi Yang:** Investigation, Resources. **Jiaheng Lin:** Methodology, Validation. **Wenjie Li:** Methodology, Validation. **Qizhan Liu:** Conceptualization, Investigation. **Cheng Cheng:** Conceptualization, Investigation, Resources, Writing – review & editing. **Jinsong Zhang:** Conceptualization, Supervision, Writing – review & editing. **Hao Wu:** Conceptualization, Supervision, Funding acquisition.

Consent for publication

Not applicable.

Ethics approval and consent to participate

The study protocol received approval from the Ethics Committee of Nanjing Medical University and Northern Jiangsu People's Hospital Affiliated to Yangzhou University.

Funding

This work was supported by the National Natural Science Foundations of China (82272244, 82402578), Jiangsu Provincial Youth Science and Technology Talents Support Project (JSTJ-2025–001), Open Research Projects of the Key Laboratory of Modern Toxicology of Ministry of Education (Nanjing Medical University).

Declaration of Competing Interest

The authors declare that they have no known competing financial interests or personal relationships that could have appeared to influence the work reported in this paper.

Acknowledgements

The authors thank Donald L. Hill (University of Alabama at Birmingham, USA), an experienced, English-speaking scientific editor for editing.

Appendix A. Supporting information

Supplementary data associated with this article can be found in the online version at doi:10.1016/j.jhazmat.2026.142316.

Data availability

Data will be made available on request.

References

[1] Munteanu, C., Popescu, C., Vladulescu-Trandafir, A.I., Onose, G., 2024. Signaling paradigms of H(2)S-induced vasodilation: a comprehensive review (Basel). Antioxidants 13.

[2] Ng, P.C., Hendry-Hofer, T.B., Witeof, A.E., Brenner, M., Mahon, S.B., Boss, G.R., Haouzi, P., Bebarta, V.S., 2019. Hydrogen sulfide toxicity: cMechanism of action, clinical presentation, and countermeasure development. J Med Toxicol 15, 287–294.
[3] Batterman, S., Grant-Alfieri, A., Seo, S.H., 2023. Low level exposure to hydrogen sulfide: a review of emissions, community exposure, health effects, and exposure guidelines. Crit Rev Toxicol 53, 244–295.
[4] Wei, S., Zhang, H., Li, H., Li, C., Shen, Z., Yin, Y., Cong, Z., Zeng, Z., Ge, Q., Li, D., Zhu, X., 2025. Establishment and validation of predictive model of ARDS in critically ill patients. J Transl Med 23, 64.
[5] Pensier, J., Fosset, M., Paschold, B.S., von Wedel, D., Redaelli, S., Braeuer, B.L.P., Novack, V., Balzer, F., Jung, B., Amato, M.B.P., Jaber, S., Talmor, D., Baedorf-Kassis, E., Schaefer, M.S., 2025. Temporal stability of phenotypes of acute respiratory distress syndrome: clinical implications for early corticosteroid therapy and mortality. Intensive Care Med.
[6] Santana Maldonado, C., Weir, A., Rumbeiha, W.K., 2023. A comprehensive review of treatments for hydrogen sulfide poisoning: past, present, and future. Toxicol Mech Methods 33, 183–196.
[7] Long, Y., Ang, Y., Chen, W., Wang, Y., Shi, M., Hu, F., Zhou, Q., Shi, Y., Ge, B., Peng, Y., Yu, W., Bao, H., Li, Q., Duan, M., Gao, J., 2024. Hydrogen alleviates impaired lung epithelial barrier in acute respiratory distress syndrome via inhibiting Drp1-mediated mitochondrial fission through the Trx1 pathway. Free Radic Biol Med 218, 132–148.
[8] Zhang, M., Shang, L., Zhou, F., Cai, Y., Wang, S., Li, J., Liu, Y., Huang, J., Yang, S., 2025. Targeting PANoptosis: a promising therapeutic strategy for ALI/ARDS. Apoptosis.
[9] Hu, L., Sun, L., Yang, C., Zhang, D.W., Wei, Y.Y., Yang, M.M., Wu, H.M., Fei, G.H., 2024. Gut microbiota-derived acetate attenuates lung injury induced by influenza infection via protecting airway tight junctions. J Transl Med 22, 570.
[10] Tang, X., Liu, J., Yao, S., Zheng, J., Gong, X., Xiao, B., 2022. Ferulic acid alleviates alveolar epithelial barrier dysfunction in sepsis-induced acute lung injury by activating the Nrf2/HO-1 pathway and inhibiting ferroptosis. Pharm Biol 60, 2286–2294.
[11] Wibbe, N., Ebnet, K., 2023. Cell Adhesion at the Tight Junctions: New Aspects and New Functions. Cells 12.
[12] Li, J., Qi, Z., Li, D., Huang, X., Qi, B., Feng, J., Qu, J., Wang, X., 2021. Alveolar epithelial glycocalyx shedding aggravates the epithelial barrier and disrupts epithelial tight junctions in acute respiratory distress syndrome. Biomed Pharm 133, 111026.
[13] Byrnes, K., Blessinger, S., Bailey, N.T., Scaife, R., Liu, G., Khambu, B., 2022. Therapeutic regulation of autophagy in hepatic metabolism. Acta Pharm Sin B 12, 33–49.
[14] Mizushima, N., Levine, B., 2020. Autophagy in Human Diseases. N Engl J Med 383, 1564–1576.
[15] Fu, Z., Wu, X., Zheng, F., Zhang, Y., 2022. Activation of the AMPK-ULK1 pathway mediated protective autophagy by sevoflurane anesthesia restrains LPS-induced acute lung injury (ALI). Int Immunopharmacol 108, 108869.
[16] Shen, Y., He, Y., Pan, Y., Liu, L., Liu, Y., Jia, J., 2024. Role and mechanisms of autophagy, ferroptosis, and pyroptosis in sepsis-induced acute lung injury. Front Pharm 15, 1415145.
[17] Chen, L.H., Wei, J.P., Li, M.D., Lu, X., Ma, Y.C., Wang, Y., Zheng, L., Fei, J., Cao, W., Xu, D.X., Yang, J., Zhao, H., Fu, L., 2025. AhR-mediated histone lactylation drives cellular senescence during benzo[a]pyrene-evoked chronic obstructive pulmonary disease. J Hazard Mater 495, 139083.
[18] Zhu, Y., Zhang, Y., Li, Y., Guo, C., Fan, Z., Li, Y., Yang, M., Zhou, X., Sun, Z., Wang, J., 2022. Integrative proteomics and metabolomics approach to elucidate metabolic dysfunction induced by silica nanoparticles in hepatocytes. J Hazard Mater 434, 128820.
[19] Paul, S., Ghosh, S., Kumar, S., 2022. Tumor glycolysis, an essential sweet tooth of tumor cells. Semin Cancer Biol 86, 1216–1230.
[20] Icard, P., Shulman, S., Farhat, D., Steyaert, J.M., Alifano, M., Lincet, H., 2018. How the Warburg effect supports aggressiveness and drug resistance of cancer cells? Drug Resist Updat 38, 1–11.
[21] Ji, Y., Xu, Z., Tang, L., Huang, T., Mu, X., Ni, C., Tang, B., Lu, H., Zhang, C., Yang, S., Wang, X., 2025. O-GlcNAcylation of YBX1 drives a glycolysis-histone lactylation feedback loop in hepatocellular carcinoma. Cancer Lett 631, 217957.
[22] Sun, K., Shi, Y., Yan, C., Wang, S., Han, L., Li, F., Xu, X., Wang, Y., Sun, J., Kang, Z., Shi, J., 2025. Glycolysis-Derived Lactate Induces ACSL4 Expression and Lactylation to Activate Ferroptosis during Intervertebral Disc Degeneration. Adv Sci (Weinh) 12, e2416149.
[23] Zhang, D., Tang, Z., Huang, H., Zhou, G., Cui, C., Weng, Y., Liu, W., Kim, S., Lee, S., Perez-Neut, M., Ding, J., Czyz, D., Hu, R., Ye, Z., He, M., Zheng, Y.G., Shuman, H. A., Dai, L., Ren, B., Roeder, R.G., Becker, L., Zhao, Y., 2019. Metabolic regulation of gene expression by histone lactylation. Nature 574, 575–580.
[24] Wang, J.H., Mao, L., Wang, J., Zhang, X., Wu, M., Wen, Q., Yu, S.C., 2023. Beyond metabolic waste: lysine lactylation and its potential roles in cancer progression and cell fate determination. Cell Oncol (Dordr) 46, 465–480.
[25] Zhang, C., Zhou, L., Zhang, M., Du, Y., Li, C., Ren, H., Zheng, L., 2024. H3K18 Lactylation Potentiates Immune Escape of Non-Small Cell Lung Cancer. Cancer Res 84, 3589–3601.
[26] Zhou, R., Li, K., Hu, X., Fan, S., Gao, Y., Xue, X., Bu, Y., Zhang, H., Wang, Y., Wei, C., Zhang, S., Xie, Z., Liu, C., Chen, P., Yin, Z., Ren, D., 2025. Sleep Deprivation Activates a Conserved Lactate-H3K18la-RORalpha Axis Driving Neutrophilic Inflammation Across Species. Adv Sci (Weinh), e04028.
[27] Geng, P., Ma, T., Xing, J., Jiang, L., Sun, H., Zhu, B., Zhang, H., Xiao, H., Wang, J., Zhang, J., 2018. Dexamethasone ameliorates H(2)S-induced acute lung injury by increasing claudin-5 expression via the PI3K pathway. Hum Exp Toxicol 37, 626–635.
[28] Hu, Y., Hu, Q., Ansari, M., Riemondy, K., Pineda, R., Sembrat, J., Leme, A.S., Ngo, K., Morgenthaler, O., Ha, K., Gao, B., Janssen, W.J., Basil, M.C., Kliment, C.R., Morrisey, E., Lehmann, M., Evans, C.M., Schiller, H.B., Konigshoff, M., 2024. Airway-derived emphysema-specific alveolar type II cells exhibit impaired regenerative potential in COPD. Eur Respir J 64.
[29] Rumbeiha, W.K., Kim, D.S., 2025. Neurological Sequelae of Acute Hydrogen Sulfide Poisoning: A Literature Review, Controversies, and Knowledge Gaps. Neurol Int 17.
[30] Pensier, J., Fosset, M., Paschold, B.S., von Wedel, D., Redaelli, S., Braeuer, B.L.P., Novack, V., Balzer, F., Jung, B., Amato, M.B.P., Jaber, S., Talmor, D., Baedorf-Kassis, E., Schaefer, M.S., 2025. Temporal stability of phenotypes of acute respiratory distress syndrome: clinical implications for early corticosteroid therapy and mortality. Intensive Care Med 51, 1784–1796.
[31] Meyer, N.J., Gattinoni, L., Calfee, C.S., 2021. Acute respiratory distress syndrome. Lancet 398, 622–637.
[32] Wick, K.D., Ware, L.B., Matthay, M.A., 2024. Acute respiratory distress syndrome. BMJ 387, e076612.
[33] Li, N., Liu, B., Xiong, R., Li, G., Wang, B., Geng, Q., 2023. HDAC3 deficiency protects against acute lung injury by maintaining epithelial barrier integrity through preserving mitochondrial quality control. Redox Biol 63, 102746.
[34] Wang, J., Zhang, H., Su, C., Chen, J., Zhu, B., Zhang, H., Xiao, H., Zhang, J., 2014. Dexamethasone ameliorates H(2)S-induced acute lung injury by alleviating matrix metalloproteinase-2 and -9 expression. PLoS One 9, e94701.
[35] Robergs, R.A., McNulty, C.R., Minett, G.M., Holland, J., Trajano, G., 2018. Lactate, not Lactic Acid, is Produced by Cellular Cytosolic Energy Catabolism. Physiol (Bethesda) 33, 10–12.
[36] Wang, H., Xia, H., Bai, J., Wang, Z., Wang, Y., Lin, J., Cheng, C., Chen, W., Zhang, J., Zhang, Q., Liu, Q., 2025. H4K12 lactylation-regulated NLRP3 is involved in cigarette smoke-accelerated Alzheimer-like pathology through mTOR-regulated autophagy and activation of microglia. J Hazard Mater 488, 137310.
[37] Panagaki, T., Pecze, L., Randi, E.B., Nieminen, A.I., Szabo, C., 2022. Role of the cystathionine beta-synthase / H(2)S pathway in the development of cellular metabolic dysfunction and pseudohypoxia in down syndrome. Redox Biol 55, 102416.
[38] Xu, K., Zhang, K., Wang, Y., Gu, Y., 2024. Comprehensive review of histone lactylation: structure, function, and therapeutic targets. Biochem Pharm 225, 116331.
[39] Sheng, X., Lin, H., Cole, P.A., Zhao, Y., 2026. Biochemistry and regulation of histone lysine L-lactylation. Nat Rev Mol Cell Biol 27, 95–109.
[40] Xiong, J., He, J., Zhu, J., Pan, J., Liao, W., Ye, H., Wang, H., Song, Y., Du, Y., Cui, B., Xue, M., Zheng, W., Kong, X., Jiang, K., Ding, K., Lai, L., Wang, Q., 2022. Lactylation-driven METTL3-mediated RNA m(6)A modification promotes immunosuppression of tumor-infiltrating myeloid cells. Mol Cell 82, 1660–1677 e1610.
[41] Gong, F., Zheng, X., Xu, W., Xie, R., Liu, W., Pei, L., Zhong, M., Shi, W., Qu, H., Mao, E., Yang, Z., Li, R., Chen, E., Chen, Y., 2025. H3K14la drives endothelial dysfunction in sepsis-induced ARDS by promoting SLC40A1/transferrin-mediated ferroptosis, 2020 MedComm 6, e70049.
[42] Shi, K., Ke, D., Li, F., Shi, R.S., Liu, T., Li, D., Zhang, Q.X., 2025. A review shows that ATG10 has been identified as a potential prognostic marker and therapeutic target for cancer patients based on real-world studies. Front Oncol 15, 1573378.
[43] Catanese, A., Olde Heuvel, F., Mulaw, M., Demestre, M., Higelin, J., Barbi, G., Freischmidt, A., Weishaupt, J.H., Ludolph, A.C., Roselli, F., Boeckers, T.M., 2019. Retinoic acid worsens ATG10-dependent autophagy impairment in TBK1-mutant hiPSC-derived motoneurons through SQSTM1/p62 accumulation. Autophagy 15, 1719–1737.
[44] Li, S., Ni, Y., Li, C., Xiang, Q., Zhao, Y., Xu, H., Huang, W., Wang, Y., Wang, Y., Zhan, J., Liu, Y., 2023. Long noncoding RNA SNHG1 alleviates high glucose-induced vascular smooth muscle cells calcification/senescence by post-transcriptionally regulating Bhlhe40 and autophagy via Atg10. J Physiol Biochem 79, 83–105.
[45] Ornatowski, W., Lu, Q., Yegambaram, M., Garcia, A.E., Zemskov, E.A., Maltepe, E., Fineman, J.R., Wang, T., Black, S.M., 2020. Complex interplay between autophagy and oxidative stress in the development of pulmonary disease. Redox Biol 36, 101679.
[46] Ryter, S.W., Lee, S.J., Choi, A.M., 2010. Autophagy in cigarette smoke-induced chronic obstructive pulmonary disease. Expert Rev Respir Med 4, 573–584.
[47] Kim, H., Wang, W., Dobrescu, I., Lee, J., Martorelli, J., Wang, S., Guo, J.Y., 2025. Autophagy in the lung: guardian of homeostasis or driver of disease. Autophagy Rep 4, 2568537.
[48] Cui, L., Yang, R., Huo, D., Li, L., Qu, X., Wang, J., Wang, X., Liu, H., Chen, H., Wang, X., 2024. Streptococcus pneumoniae extracellular vesicles aggravate alveolar epithelial barrier disruption via autophagic degradation of OCLN (occludin). Autophagy 20, 1577–1596.
[49] Xiong, X., Dou, J., Shi, J., Ren, Y., Wang, C., Zhang, Y., Cui, Y., 2023. RAGE inhibition alleviates lipopolysaccharides-induced lung injury via directly suppressing autophagic apoptosis of type II alveolar epithelial cells. Respir Res 24, 24.
[50] Sun, W., Jia, M., Feng, Y., Cheng, X., 2023. Lactate is a bridge linking glycolysis and autophagy through lactylation. Autophagy 19, 3240–3241.
[51] Li, W., Zhou, C., Yu, L., Hou, Z., Liu, H., Kong, L., Xu, Y., He, J., Lan, J., Ou, Q., Fang, Y., Lu, Z., Wu, X., Pan, Z., Peng, J., Lin, J., 2024. Tumor-derived lactate promotes resistance to bevacizumab treatment by facilitating autophagy enhancer

protein RUBCNL expression through histone H3 lysine 18 lactylation (H3K18la) in colorectal cancer. Autophagy 20, 114–130.
[52] Xu, L., Ye, Y., Gu, W., Xu, X., Chen, N., Zhang, L., Cai, W., Hu, J., Wang, T., Chao, H., Tu, Y., Ji, J., 2025. Histone lactylation stimulated upregulation of PSMD14 alleviates neuron PANoptosis through deubiquitinating PKM2 to activate PINK1-mediated mitophagy after traumatic brain injury. Autophagy 21, 1473–1491.
[53] Zhao, J., Liu, X., He, Y., Sun, Q., Xue, Z., Tang, Z., Liu, J., Wang, J., Li, C., Wang, X., Yang, N., Qiu, C., 2026. Histone H4K8 lactylation promotes glioblastoma progression by inducing NUPR1-mediated autophagosome-lysosome fusion. Theranostics 16, 4427–4451.
[54] Frisch, A.T., Wang, Y., Xie, B., Yang, A., Ford, B.R., Joshi, S., Kedziora, K.M., Peralta, R., Wilfahrt, D., Mullett, S.J., Spahr, K., Lontos, K., Jana, J.A., Dean, V.G., Gunn, W.G., Gelhaus, S., Poholek, A.C., Rivadeneira, D.B., Delgoffe, G.M., 2025. Redirecting glucose flux during in vitro expansion generates epigenetically and metabolically superior T cells for cancer immunotherapy. Cell Metab 37, 870–885 e878.
[55] Joseph, S., Sharma, A., Horne, L.P., Wood, C.E., Langaee, T., James, M.O., Stacpoole, P.W., Keller-Wood, M., 2020. Pharmacokinetic and Biochemical Profiling of Sodium Dichloroacetate in Pregnant Ewes and Fetuses. Drug Metab Dispos 49, 451–458.
[56] Chen, J., He, J., Wang, X., Bai, L., Yang, X., Chen, J., He, Y., Chen, K., 2025. Glis1 inhibits RTEC cellular senescence and renal fibrosis by downregulating histone lactylation in DKD. Life Sci 361, 123293.
[57] Jiao, Q., Ren, Y., Teng, X., Feng, M., Liu, X., Cai, Y., Hu, T., Wang, M., Wang, Y., 2025. Positive feedback between histone H4K16 lactylation and glycolysis promotes MAFLD progression. Hepatol Int.